J Comput Aided Mol Des (2009) 23:321–332
DOI 10.1007/s10822-009-9262-7

Computational study of the heterodimerization between μ and δ receptors

Xin Liu · Ming Kai · Lian Jin · Rui Wang

Received: 30 August 2008 / Accepted: 18 January 2009 / Published online: 13 February 2009

Abstract A growing body of evidence indicated that the G protein coupled receptors exist as homo- or heterodimers in the living cell. The heterodimerization between μ and δ opioid receptors has attracted researchers' particular interests, it is reported to display novel pharmacological and signalling regulation properties. In this study, we construct the full-length 3D-model of μ and δ opioid receptors using the homology modelling method. Threading program was used to predict the possible templates for the N- and C-terminus domains. Then, a 30 ns molecular dynamics simulations was performed with each receptor embedded in an explicit membrane-water environment to refine and explore the conformational space. Based on the structures extracted from the molecular dynamics, the likely interface of μ–δ heterodimer was investigated through the analysis of protein–protein docking, cluster, shape complementary and interaction energy. The computational modelling works revealed that the most likely interface of heterodimer was formed between the transmembrane1,7 (TM1,7) domains of μ receptor and the TM(4,5) domains of δ receptor, with emphasis on μ-TM1 and δ-TM4, the next likely interface was μ(TM6,7)-δ(TM4,5), with emphasis on μ-TM6 and δ-TM4. Our results were consistent with previous reports.

Keywords GPCR heterodimerization · Opioid receptors · Protein–protein docking · Homology modelling · Molecular dynamics simulations

Introduction

G protein-coupled receptors (GPCR) are the largest superfamily in the human genome and more than 4,000 GPCRs have been sequenced [1]. GPCRs have been classified into five distinct groups (GRAFS) based on phylogenetic analyses of sequences from the human genome [2]. Such receptors are activated by a diverse array of stimuli including amines, peptides, lipids, nucleotides, odors, tastes and photons of light and involved in essential cell recognition and communication processes [3]. Owing to their critical role in physiological processes, GPCRs are involved in all major disease areas, including cardiovascular, metabolic, neurodegenerative, psychiatric, cancer and infectious diseases [4, 5]. It is estimated that nearly 60–70% of drugs in development today target 20 GPCRs, and 26 out of the top 100 selling drugs target members of the GPCR family [6–8].

Classically, GPCRs had been considered to be expressed, exist and function as monomeric unit and the model of ligand binding and signal transduction by GPCRs were also based on this assumption, however, this idea has been challenged over the past few years. The growing biophysical

Electronic supplementary material The online version of this article (doi:10.1007/s10822-009-9262-7) contains supplementary material, which is available to authorized users.

X. Liu · M. Kai · L. Jin · R. Wang (✉)
Institute of Biochemistry and Molecular Biology, School of Basic Medical Science, State Key Laboratory of Applied Organic Chemistry, Lanzhou University, 222 Tianshui South Road, 730000 Lanzhou, China
e-mail: wangrui@lzu.edu.cn; liux_05@lzu.cn

R. Wang
State Key Laboratory of Chinese Medicine and Molecular Pharmacology, Department of Applied Biology and Chemical Technology, The Hong Kong Polytechnic University, Kowloon, Hong Kong, China

and biochemical evidence suggests that many GPCRs form functional homodimers or heterodimers [9–20]. Early studies using radioligand binding, cross-linking and radiation inactivation had predicted the oligomerization of GPCRs [21], since the middle of 1990s, studies facilitated by co-immunoprecipitation, Cellular Fluorescence or Bioluminescence Resonance Energy Transfer (FRET and BRET) also revealed many GPCRs exist as dimers [15, 22–25]. Recently, the work by Placzewski showed that most rhodopsin and opsin molecules form constitutive dimers in dark adaptive retinal membrane, indicating perhaps the clearest demonstration of GPCR dimerization [26, 27]. Studies have shown that dimerization occurs early after biosynthesis, and is necessary for correct transport of receptor to the plasma membrane, indicating that it plays a primary role in the protein maturation [20, 28]. Pharmacological and signal transduction experiments now suggest that the dimerization of GPCRs could be important for regulation of their pharmacology and signaling [14–18, 20, 24].

The opioid receptors, belonging to the subfamily A of GPCR, are comprised of three cloned subtypes: μ, δ and κ [29]. These receptors are extremely important clinical targets in the treatment of pain and additionally have profound effects on the neuroendocrine system and immune response [30]. It was reported that opioid receptors can form homodimers and heterodimer within its own family, heterodimers have been reported between δ receptor and κ opioid receptor, μ and δ opioid receptor [31–34]. And it is interesting that the heterodimerized opioid receptors have different pharmacological profiles and receptor trafficking properties from the monomers: the κ–δ heterodimer exhibit decreased affinities for either κ or δ selective ligands alone, but the heterodimer synergistically binds certain partial selective ligands with high affinity [34]. The μ–δ heterodimer exhibit the similar altered binding profile [32, 33]. Specifically, many studies suggest that certain δ antagonist was able to increase the level of μ receptor agonist-mediated signaling significantly when the two receptors co-expressed [35–40]. This finding is of particular interest, because these data indicates not only the interaction between the μ opioid receptor and δ opioid receptor modulates the μ-mediated tolerance and dependence, but also provides probably another available way for developing potent analgesia drug devoid of tolerance and dependence, posed by single μ agonist treatment. Clearly, it would be most useful to have the 3D structures of the monomer and heterodimer to help study the mechanism of the new pharmacology.

However, because of the technical difficulty and of large-scale receptor purification and the insolubility in media lacking phospholipid, there are no available 3D structures of opioid receptors determined by X-ray or NMR studies. Fortunately, the X-ray structure of bovine rhodopsin was solved at 2.2 Å resolution [41], this structure has been widely applied to homology modelling, based on the hypothesis of structural mimicry [42], GPCRs are characterized structurally by a heptapeptidic transmembrane helix connected by three extracellular and intracellular loops, an N-terminal and a cytoplasmic C-terminal domain [43]. The 7TM domains are known to adopt common folding pattern, and thus the 7TM domains constitute the most conserved domain across the GPCR. Several highly conserved structural motifs are known to be presented in the 7TM bundle of Class A GPCRs [44, 45], like, the "D/ERY" motif at the end of the TM3, the TM6 "aromatic cluster" motif, the "NPXXY" motif at the end of TM7, and so on. Thus, it can be reasonably to construct the 3D models of transmembrane bundles of opioid receptors, using homology modelling techniques based on the X-ray structure of bovine rhodopsin as the structural template. Another difficulty for building up the opioid receptor structure is that the length of the N and C terminus of bovine rhodopsin is not appropriate for that of the opioid receptors, new templates are needed for these domains.

In general, there are two methods can help to predict the protein–protein interface, sequence methods and docking methods [46–50]: if structural information about the interacting proteins is not available, methods based on sequence and genomic information can be used to predict probable domains involved in protein–protein interactions. If the atomic structures of the individual proteins involved in an interaction are known, either by experiment or by computational modelling, the structure of the interaction can be suggested by the docking methods.

In the present study, the protein–protein docking method had been used in prediction the domains likely involved in the μ–δ heterodimer. The μ and δ receptors were constructed by the homology modelling method, the latest X-ray structure of bovine rhodopsin was used as template for the transmembrane bundle of the receptors. The template for each terminus domain of the two receptors was predicted by the optimal sequence threading method [51]. The generated structure models were further optimized by nanosecond scale molecular dynamics (MD) simulations in explicit membrane-water environment. Rigid-body protein–protein dockings were performed using the structures extracted from the MD simulations. Then the docking poses were clustered to different groups and filtered, finally the interaction energy of the representative structures were calculated and used as a major criterion to identify the possible contact pattern between the μ and δ opioid receptors.

Materials and methods

Homology modelling

The whole sequences of μ and δ receptor (Swiss-Prot entry P35372 and P41143) were used to build up the 3D structures of both receptors by means of MODELLER 9V2 [52]. Sequence alignment was carried out using the software ClustalW [53]. For the μ receptor, the X-ray structure of bovine rhodopsin (PDBID = 1U19) was used as the template for the transmembrane and loop domains, except the intracellular loop 3 and extracellular loop 3. The templates for C-terminus and N-terminus were determined by the programs THREADER [51] and PSI-Pred [54]. THREADER and PSIPRED achieved very good score in the previous CASP experiments [55–57], and these methods have been reported to be used in building up the long loops of GPCR models [9, 58]. We had also tested some other programs, including HMM-TOP [59, 60], TOPPRED [61, 62] and TMPRED [63], on bovine rhodopsin, we found that the THREADER and PSIPRED combination had better prediction results. After several THREADER runs with different parameters, the reliable results of z-score above 3.5 were collected and filtered by the following rules: (1) as to the identity and similarity between the template and the target sequence, the higher the better, (2) as to the gaps in each alignment mode, the less and the shorter the better, (3) appropriate space orientation was needed, e.g., do not violate the transmembrane bundle. Two separate templates, indicated by their PDBID hereinafter, 1K1G (137–186 of chain A) and 2ENK (30–72) were finally selected for N-terminus and C-terminus, respectively. Structural homologs of sequences in the intracellular loop 3 (IC3) and extracellular loop 3 (EC3) were obtained by searching the PDB database [64] using PSI-BLAST [65] with either PAM30 or PAM70 matrices. Structure 2QRU (231–245) was used as templates for the EC3, 1J5Y (20–34) was used as templates for IC3. The model of δ receptor was built similarly with 1CEE (15–44 of chain A), 2E71 (760–792), 2DPW (222–232), 1ZUY (34–47) for the N-terminus, C-terminus, EC3 and IC3, respectively. The structures of previous mentioned templates were obtained from the Protein Data Bank. Using the homology modelling program MODELLER, 1,000 structures were generated for each receptor, which were clustered into five different groups with respect of the variation of Cα deviation. The model with the highest PROCHECK [66] score from each group was selected and subject to MDS filter. After the energy minimization and short MD simulations in vacuo, the structure with the lowest energy was considered as the best result.

Setup for the explicit membrane-water environment

An explicit membrane-water environment was considered in the simulations of both monomers and heterodimers. The pre-equilibrated dipalmitoylphosphatidylcholine (DPPC) bilayer with extended water layers was used in all dynamic simulations. The structure files for DPPC bilayer were downloaded from Dr. Tielman's website (http://moose.bio.ucalgary.ca). For μ receptor model, the explicit membrane-water system consisted of 400 amino acid residues, 100 DPPC lipid molecules, 7 chloride counter ions, and 6821 SPC water molecules, altogether a total of 29,487 atoms. For δ receptor, the system consisted of 372 residues, 100 DPPC lipid molecules, 13 chloride counter ions, and 6,915 SPC water molecules, altogether of 29,374 atoms. The dimensions of the central unit cell were approximately $70 \times 70 \times 99$ Å. The initial DPPC bilayer was duplicated and truncated so that it could accommodate the models of μ–δ heterodimers. Finally, the heterodimer models were embedded in a $122 \times 122 \times 99$ Å unit cell, with average of 360 lipid molecules, 26,430 water molecules, and 20 chloride counter ions.

Molecular dynamics simulations

Molecular dynamics simulations were performed using the GROMACS package [67], using NPT and periodic boundary conditions. A modification of GROMOS87 force field [68] was applied for protein and the lipid parameters adopted were the same as the previous MD studies of lipid bilayers [69–71]. A twin cutoff of of 9Å was used for the short range interaction and a cutoff of 12Å was used for the Lennard-Jones interaction. Particle Mesh Ewald algorithm [72] was used for the calculation of electrostatic contributions to energies and forces. The neighbor list was updated every ten steps. Bond length was constrained using the LINCS algorithm [73]. The systems were coupled to a temperature bath at 300 K, with a coupling constant of 0.1 ps [74]. Semi-isotropic coupling with time constant of 1 ps was applied to keep the pressure at 1.0 bar [74].

The dynamics simulations of both monomer and heterodimer system were first energy minimized using a steepest descent algorithm followed by conjugated gradient algorithm until a convergence of 100 kJ mol^{-1} $Å^{-2}$ was reached. Then a progression of position restraint was performed. First, only hydrogen atoms could move for 40 ps, second, only the side chains of terminus domains and loops could move for 80 ps, then, only the transmembrane bundle was fixed for 120 ps, at last, only the backbone of the helixes were kept fixed and gradually released during 160 ps. After these dynamics simulations to gradually release all the constraints in each system, another 30 and

5 ns of MD simulations were conducted for each monomer and heterodimer, respectively.

Protein–protein docking

Prediction of heterodimer structures was done by means of the rigid-body docking program ZDOCK2.1 [75]. 56 structural conformations were collected for each receptor from the MDS (every 400 ps since 8 ns and the average structure of 0–8 ns). The μ receptor was first treated as the fixed target protein, δ receptor as probe protein, and then the two receptors changed their roles, with δ receptor fixed and μ receptor moved as probe, with 120 docking runs totally getting involved. A rotational sampling interval of 60 was employed and the top 4,000 solutions, ranked by ZDOCK score, were maintained for each run. The filtering of the models was performed by FiPD according to MemTop definition [76], with the thresholds of 0.4 rad for the tilt angle and 6.0 Å for the z-offset, respectively. This filter discards all the solutions that violate the membrane topology, characterized by a deviation angle from the original z-axis (tilt angle), and a displacement of the geometrical center along the z-axis (z-offset). MemTop $= \sqrt{(\text{tilt}_{\text{nor}})^2+(Z_{\text{offnor}})^2}$, ($\text{tilt}_{\text{nor}}$) and ($Z_{\text{offnor}}$) are the normalized tilt angle and the z-offset averaged over all the members of a given cluster. The optimal value for this calculation is zero. The benchmark of this docking protocol used in our study was reported previously on several transmembrane oligomers with known structure [76], the results shown that this was an effective strategy to predict the organization of supramolecular. The interaction residues between the two receptors were calculated with a maximum distance of 4.5 Å, contact surface area values were calculated using probe radius of 1.4 Å [77]. The figures were drawn by means of PyMol [78].

Results and discussion

Sequence alignment and homology modelling

In this work, we constructed the 3D structure of both μ and δ opioid receptor with the full query of sequences by deploying the homology modelling protocol. In the meantime, bovine rhodopsin was introduced as the template for the transmembrane domains. When we were starting our current work, the crystal structure of the human beta2-adrenergic receptor was reported. Comparing with the bovine rhodopsin 3D structure, the structure of beta2-adrenergic receptor showed a more open structure especially in the extracellular loop 2 and the lower ends of TM3 and TM6 [79]. We've tried to construct our models using the crystal structure of beta2-adrenergic receptor as template, in which case, we had to manually adjust the sequence alignment to maintain the highly conserved disulfide bond between TM3 and ECL2, and this manual adjustment would result a long consecutive gap in ECL2. However, if the bovine rhodopsin was chosen as the template, the conserved disulfide bond could be correctly aligned using ClustalW with no artificial interference. For another major structure difference in TM3 and TM6, the author suggested that this feature could be the basis for the basal activity observed for many GPCR [80]. Because the current work only deals with the heterodimerization between two GPCRs and does not concern the dynamics of activations, the presented models based upon bovine rhodopsin are, in our opinion, still valid. The bovine rhodopsin structure has been widely used as a template to generate relevant GPCR homology models [81], the resolution of the other GPCR crystal structures does not fade the usefulness of the rhodopsin crystal structure serving as a reliable template for building relevant 3D models of other GPCRs.

In realizing that accurate alignment was of utmost importance in building up a useful 3D homology model, so multiple sequences of Class A GPCRs were used during the alignment process to minimize the errors when single template used. Though, the overall homology of these GPCRs was very low, the TM domains of our receptors had higher percentage of identity to rhodopsin than the average value of the whole protein, and there were some highly conserved key residues among them(supporting information S1 and S2), including Asn55 in TM1 (numbered according to bovine rhodopsin, hereinafter), Asp83 in TM2, the conserved disulfide bond (linking Cys110 and Cys187) and Arg135 (within the D/ERY motif) in TM3, Trp161 in TM4, Pro216 in TM5, Pro267 in TM6 and Pro303 (within the NPXXY motif) in TM7. These highly conserved residues can be used as reference points for each helix during the alignment (Fig. 1).

Since the opioid receptors had much longer N and C terminus than that of bovine rhodopsin, the identity of these domains were significantly low, and two loop domains, intracellular loop 3 (IC3) and extracelluar loop 3 (EC3), also had very low percentage of sequence identity with rhdoposin, so proper templates were needed to construct these domains. The templates for the two loop domains were obtained by searching the PDB database, and special attention were paid to the terminus domains. Here we employed the fold recognition program THREADER and secondary structural prediction program PSI-PRED to predict the templates for the terminal domains. We carried out many prediction runs with different sets of parameters with the emphasis on either sequence similarity or secondary structure prediction, and got 2–5 results for each terminus. According to the protocol describe in the methods sections,

Fig. 1 Alignments between the three opioid receptors and bovine rhodopsin (*BRho*). The transmembrane domains (*TM1-TM7*) are colored in *cyan*, the loops and Helix8 (EC1-EC3, IC1-IC3 and H8) are colored in *pink*. The conserved positions are indicated by *black*. The *red shaded* domains are the fragments that have been modelled without use of the BRho structure (N-terminus, C-terminus, EC3 and IC3)

four templates were finally selected for building up the terminal domain, splicing factor 1 (137–186) and putative DNA-binding domain of zinc transporter protein (30–70) for construct the N and C terminus of μ receptor, respectively, GTPase binding domain of wiskott–aldrich syndrome protein (15–44) and FF domain of transcription elongation regulator 1 (760–792) for those of δ receptor, correspondingly (suppotring information S3 and S4). By the means of MODELLER and molecular dynamics filter, the best structural model for each receptor was selected. PROCHECK was used to calculate the phi and psi angles for the two remaining models. The Ramachandran plot showed that (Fig. 2), for μ receptor, 97.3% of the residues were found in the most favored region and in the additional allowed region. Only two residues, which located in the intracellular loops, were found in the disallowed region. For δ receptor, 98.1% of the residues were found in the two allowed regions and no residues were found in the disallowed region. These data indicated that the two homology models had good stereochemistry properties.

Molecular dynamics refinement of the two monomers

To further optimize the structures and present them in a more natural way, MD simulations were performed with the two receptors embedded in explicit membrane-water environment. In this process, the receptor structures were first minimized, then subjected to the position restraint simulations, during the 400 ps constraint simulations, the position restraints were gradually released so as to refine the structure. Finally, two 30 ns MDS without any manual perturbation were performed. At the same time, to examine the variations of the protein conformations and stability of the systems, the root-mean-squared deviation (rmsd) with respect to the initial structures were calculated. Figure 3 showed the rmsd for Cα of the receptors as a function of the simulation time, we can see the two receptors experienced similar structure fluctuation changes through the whole simulation: after the initial Cα rmsd increase in the magnitude of residue fluctuation during the first 8.5 ns, μ and δ receptors reached a plateau at about 3 and 4.5Å for the rest of the simulation. The potential energy of the two systems also became stable after the first 8.5 ns simulation (supporting information S5). Analysis of the MD simulations trajectory for both of the receptors showed that some important structure features and conserved interactions as reported previously were stabilized or formed spontaneously. Take μ opioid receptor for example, the highly conserved residue ASP116(2.50) (numbers in parentheses followed Ballesteros and Weistein's numbering convention [82], where the first number indicated the helix and the second number associated with the position relative to the most conserved residue in that helix, which was denoted as 50) formed a intramolecular hydrogen bonding network between the highly conserved ASN88(1.50) and SER331(7.46), as was observed in bovine [83]. ASN166(3.49) in the highly conserved "DRY" motif formed a salt bridge with the ARG167(3.50), which was also associated with THR281 (6.34) in the conserved "XBBXXB" motif ('B' represents a basic residue, 'X' represents a non-basic residue). These ionic interactions played a critical role in governing receptor activation [84, 85]. The highly conserved disulfide bond between TM3 and EC2 was maintained throughout the MD simulations [43]. PHE291(6.44) and TRP295(6.48) in the highly conserved "aromatic cluster" motif contacted with each other in a π-staking arrangement, which was considered to stabilize the inactive conformation of the receptor [86, 87]. TYR338(7.53) in the highly conserved "NPXXY" motif was involved in a aromatic interaction with PHE345(7.60), this TM7-Helix8 interaction was considered

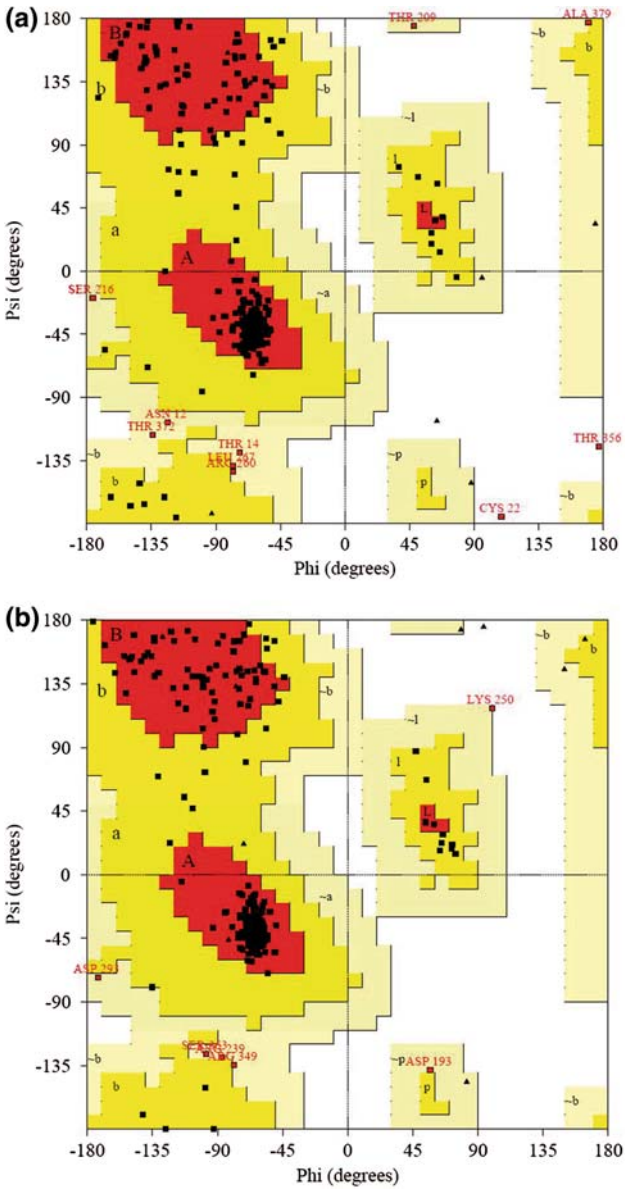

Fig. 2 Ramachandran plot for the two selected models produced using the programs PROCHECK. μ receptor is on the *top* (**a**), δ receptor is on the *bottom* (**b**)

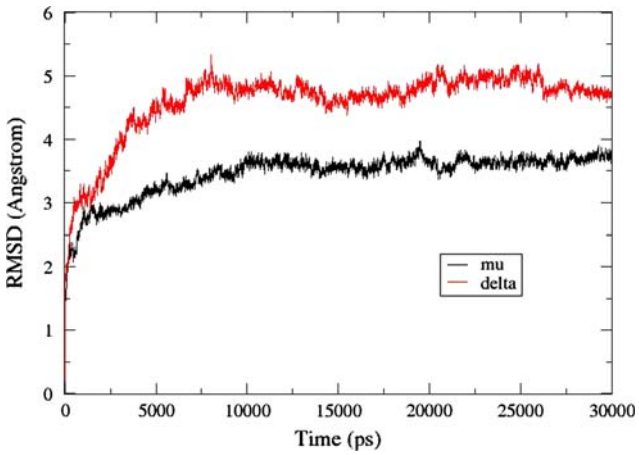

Fig. 3 Simulation time versus rmsd of the Cα of the system with μ (*black*, *bottom*) and of the system with δ (*red*, *top*) receptor

to play a significant role in controlling the activation state of GPCR [45, 83]. The δ opioid receptor shared the same residues and structure characteristics with μ opioid receptor in the above mentioned conserved motifs. These results suggest that the two systems were well equilibrated through the MD simulations and suitable for the protein–protein docking study.

Rigid protein–protein docking

The rigid body protein–protein dockings were performed using the Fast Fourier Transform-based algorithm program ZDOCK. The docked conformations of the monomers were collected from the 30 ns MD simulations (see computational methods section). After the first round of dockings, 224,000 solutions altogether were ranked by the ZDOCK scoring function. However, not all of these solutions were ideal for our case. As we know, for the rational orientation of the GPCRs, their *z*-axis should be generally perpendicular to the water/lipid interface of the membrane, and when they exist as dimers in the membrane environment, the line across the geometrical center of transmembrane of each receptor should be generally parallel to the water/lipid interface [76].

The docked solutions were further filtered, according to this membrane topology, only 2,601 models were left and ranked by the MemTop score, and the top 30% (781 models) were collected for detailed analysis. Automatic cluster were then performed, divided the remaining structures to 21 groups. The automatic clustering was performed with ClusPro, which is based on the Fourier correlation algorithm and ranking the results by their clustering properties [88]. Special attention was paid for the TM domains. After statistical examination of the data and visual observations over the structures, we found that, in many cases there were mainly two TM domains involved in the interface, and we defined the contact pattern of our heterodimers by their contact TM. Four contact patterns with the largest number of population were then discovered, the average numbers of contact residues for each TM were also calculated (Table 1). As we can see from the Table 1, μ(TM6,7)–δ(TM4,5) dimers constituted the largest group, accounting for 28% of the total population, and the residues came from μ-TM6 and δ-TM4 were much more than the other two TM domains indicated that the contact between μ-TM6 and δ-TM4 may be more significant. The second largest group came from the μ(TM1,7)–δ(TM4,5) interaction, accounting for 26% of the population, with 2% less than the first

Table 1 Average number of residues that participated in the interface for each contact pattern

Contact pattern	μ Receptor		δ Receptor	
	Domain	Number	Domain	Number
μ(TM1,7)–δ(TM4,5)	TM1	17	TM4	18
	TM7	12	TM5	8
μ(TM6,7)–δ(TM4,5)	TM6	12	TM4	15
	TM7	8	TM5	7
μ(TM1,2)–δ(TM1,7)	TM1	11	TM1	8
	TM2	8	TM7	3
μ(TM4,5)–δ(TM4,5)	TM4	10	TM4	16
	TM5	13	TM5	8

pattern, and μ(TM1)–δ(TM4) interaction was more significant. μ(TM4,5)–δ(TM4,5) pattern accounting for 16% of the population, it was much less than the previous two patterns, the μ(TM5)–δ(TM4) interaction may play an important role for this kind of interface. The μ(TM1,2)–δ(TM1,7) pattern accounted for 10%, here the main contact was the interaction between the two TM1 helixes. The population of each of the rest 17 groups accounted for no more than 5% of the total number, respectively, so they were neglected for the further investigation.

Structural candidates of μ–δ heterodimer

In a more recently study, the truncation experiments performed on both μ and δ receptor suggested that the interaction between the two receptors involved the distal carboxyl tail of both receptors as crucial elements necessary for generating the novel pharmacological profile of the heterodimer [50, 89]. Among our selected four contact patterns, the C-terminus of μ(TM1,2)–δ(TM1,7), μ(TM1,7)–δ(TM4,5) and μ(TM6,7)–δ(TM4,5) tended to approach to each other, measuring the contact surface area also indicated there were interactions between the two domains (Table 2). The μ(TM4,5)–δ(TM4,5) dimer had larger contact surface area in the TM domain, however, because of the interface location, the two C-terminus of μ(TM4,5)–δ(TM4,5) model lay at the opposite directions of the interface, making it difficult for the two domains to contact with each other. The μ(TM1,2)–δ(TM1,2) models had close contact in the terminus domains, but they had much less contact in the very conserved TM domains. It seems that the μ(TM1,7)–δ(TM4,5) and μ(TM6,7)–δ(TM4,5) models may be more consistent with the previous findings. μ(TM6,7)–δ(TM4,5) dimer had the largest contact area of 3,252 Å^2, μ(TM1,7)–δ(TM4,5) dimer had the next largest contact area of 3,240 Å^2, the difference of contact surface area between the two dimers were very small.

Table 2 Average contact areas for the four kinds of contact dimers (Å^2)

Contact pattern	Protein–protein	TM–TM	Cterm–Cterm
μ(TM1,7)–δ(TM4,5)	3,240	2,029	440
μ(TM6,7)–δ(TM4,5)	3,252	2,220	435
μ(TM1,2)–δ(TM1,7)	2,040	460	655
μ(TM4,5)–δ(TM4,5)	2,440	2,290	0

Interaction energy calculation

In our protein–protein docking study, the monomers were treated as rigid-body, the flexibility and possible structure changes during the docking process were therefore neglected. Also, some atomic clashes or bad contacts may be generated during the rigid-body docking. According to the recent report, the quality for the large rigid-body docked complexes with interface area >1,500 Å will benefits a lot from the MD relaxation [90]. Therefore, to further screen the four docked candidates, we selected two models from each contact pattern based on their ZDOCK scores, and they were first energy minimized to a local minimum, then followed by 5 ns MD simulations in explicit membrane-water system (Fig. 4; supporting information S6). Then the interaction energy was calculated as the major criteria to rank the poses. Finally, we found two contact patterns may be more favored for the energy perspective.

The average interaction energies were listed in Table 3. As we can see, the μ(TM1,7)–δ(TM4,5) interaction pattern probably was the most energetically favorably model, its

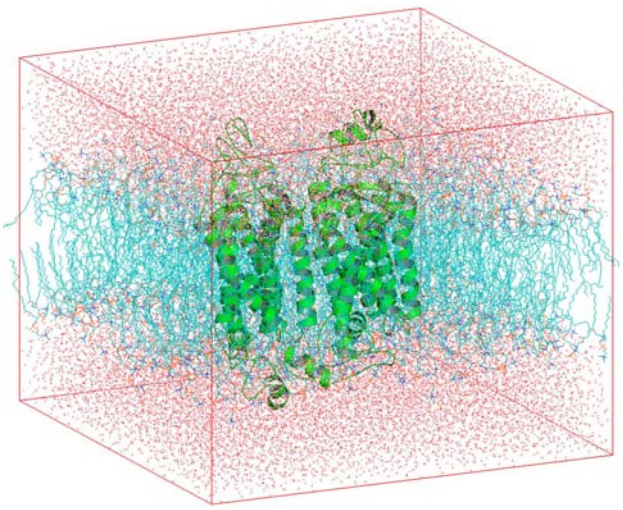

Fig. 4 Representation of the heterodimer model in the explicit membrane-water system with periodic boundary conditions. The proteins, DPPC bilayer and water are colored in *green*, *cyan* and *red*

Table 3 Average interaction energy of the four contact dimers

Contact pattern	Elec energy	vdW energy	Total energy
μ(TM1,7)–δ(TM4,5)	−495	−1235	−1730
μ(TM6,7)–δ(TM4,5)	−450	−1180	−1630
μ(TM1,2)–δ(TM1,7)	−250	−580	−830
μ(TM4,5)–δ(TM4,5)	−190	−790	−980

The table shows the electrostatic, the van der Waals and the total energy (kJ mol^{-1})

interaction energy was lowest among the four contact patterns. In 2003, by a new subtractive correlated mutation method, Filizola and Weinstein et al. had predicted the likely heterodimerization interface of the μ–δ pair involves TM4, TM5 and TM6 of the δ receptor with TM1 of the μ receptor [91], our μ(TM1,7)–δ(TM4,5) contact dimer (Fig. 5a, b; supporting information S7) was in agreement with this sequence-based prediction. The next energetically favorably model was μ(TM6,7)–δ(TM4,5) (Fig. 6a, b; supporting information S8), which constituted the group with the largest number of population, its average interaction energy was about 100 kJ mol^{-1} (23.9 kcal mol^{-1}) bigger than the μ(TM1,7)–δ(TM4,5) contact dimer. However, for the rest two kinds of contact dimer, their interaction energy were much bigger than the previous two models, which indicated that these two kinds of contact pattern may not be preferred by the energy. With regards to the above mentioned results, μ(TM1,7)–δ(TM4,5) contact dimer held the most energetically favorable interface and the largest size of surface contact area, this contact dimer probably represented the most favorable contact between the two monomers. μ(TM6,7)–δ(TM4,5) contact dimer were considered as the next favorable contact dimer, although it had slightly larger number of population than the μ(TM1,7)–δ(TM4,5) contact dimer.

It is clear that comparing the two components of the interaction energy, the vdw contact probably played a more important role than the electrostatic contact, this indicates that our contact dimers had more hydrophobic residues contact with each other. This was consistent with the Jones and Thornton's work, they analyzed 25 solvable heterocomplexes with different size and found that the large hydrophobic and uncharged residues were more frequent in the interface of heterocomplexes, the charged residue more frequent in exposed, noncontact surface [92, 93].

The detailed interactions of μ(TM1,7)–δ(TM4,5) and μ(TM6,7)–δ(TM4,5) contact dimers were analyzed based on the refined structures of previous MDS (average structures of 2–5 ns). For each contact pattern, there were two refined structure, only the interactions appeared in both of the structures were of interest. In general, these interactions were thought to have higher frequency to appear in the interface and might represent the "core" contacts between

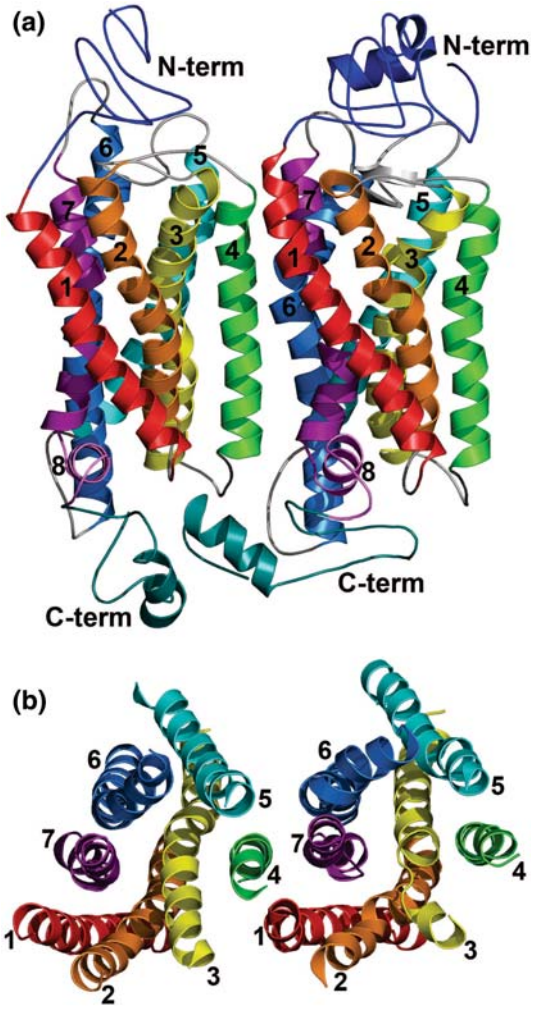

Fig. 5 Side view (**a**) and top view, seen from the extracelluar side (**b**) representations of the μ(TM1,7)–δ(TM4,5) model of μ–δ heterodimer. δ receptor is on the *left*, μ receptor is on the *right*. The loops, N-terminus and C-terminus are respectively colored in *gray*, *blue* and *deep-teal*, the three domains are not shown in top view. TM1, TM2, TM3, TM4, TM5, TM6, TM7 and Helix8 are, respectively, colored in *red*, *orange*, *yellow*, *green*, *cyan*, *marine*, *purple* and *violet*. Terminus domains, loops and helix8 are neglected in **b**

the two monomers. In our study, the electrostatic interactions were calculated by the PME algorithm, two residues were considered to be in contact if the distance between the charged atoms was <9 Å (Table 4). For hydrogen bonds, the cutoff for the angle (Acceptor–Donor-Hydrogen) and the distance (acceptor-hydrogen) were set to 30° and 3.5 Å, respectively (Table 5). For hydrophobic interaction, we calculated the distance between a carbon atom and the closest hydrophobic part of the other residue, a cutoff of 4.5 Å was used (Table 6). We can see that the TM domains contributed a lot to the hydrophobic interactions, and the electrostatic interactions occured mainly in the cytoplasmic domains of the contact dimers. In fact, previous mutagenesis experiments revealed that Glu390 and Glu395 of μ

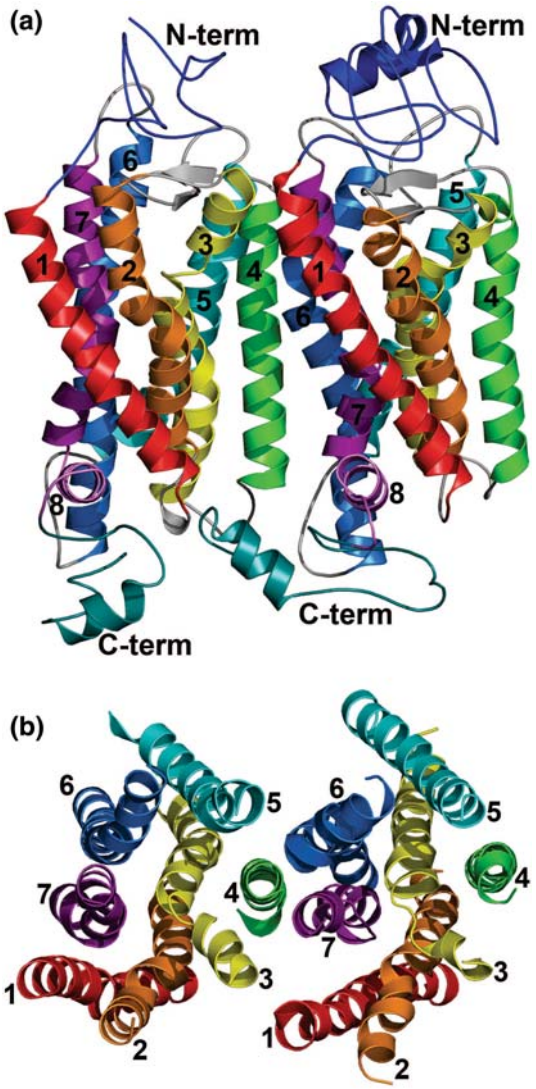

Fig. 6 Side view (**a**) and top view (**b**), seen from the extracelluar side) representations of the μ(TM6,7)–δ(TM4,5) model of μ–δ heterodimer. δ receptor is on the *left*, μ receptor is on the *right*. The loops, N-terminus and C-terminus are respectively colored in *gray*, *blue* and *deep-teal*, the three domains are not shown in top view. TM1, TM2, TM3, TM4, TM5, TM6, TM7 and Helix8 are, respectively, colored in *red*, *orange*, *yellow*, *green*, *cyan*, *marine*, *purple* and *violet*. Terminus domains, loops and helix8 are neglected in **b**

opioid receptor is important for the receptor internalization, in μ(TM6,7)–δ(TM4,5) contact dimer μ-Glu390 formed a saltbridge with δ-Arg160, and this residue was also invovled in the electrostatic contacts with both μ-Glu390 and μ-Glu395 in μ(TM1,7)–δ(TM4,5) contact dimer.

Linkage to known experiments

Despite intensive experimental investigations, the information about the GPCR dimerization interface is still rather limited, and most of these studies were restricted to homodimerization. Based on the spatial arrangement of rhodopsin observed by AFM, an atomic model of rhodopsin homodimers and higher-order oligomers has been proposed [26]. Accordingly, the intradimeric contacts have been shown to symmetrically involve both TM4 and TM5. However, rhodopsin crystal structures under different crystallization conditions leaded to alternative dimeric arrangement, which was compatible with the AFM images [94]. These homodimers featured symmetric interface involving TM1, TM2 and H8. Symmetric cysteine cross-linking experiment of dopamine D2 receptor suggested that the TM4 was involved in the homodimer interface [95]. In fact, using co-immunoprecipitation and Bioluminescence Resonance Energy Transfer (BRET) techniques, the 5-HT4R homodimer was considerably decreased under reducing condition, the author suggested that intracellular disulfide bridges between TM3 and TM4 are specifically involved in the 5-HT4R homodimerization interface [96]. The disulphide-trapping experiments on 5HT2c serotonin receptor indicated two homodimer interfaces: a quasisymmetrical TM4/5 interface which is sensitive to the activation state of receptor and a symmetric TM1 interface insensitive to the activation state [97]. Collectively, this data suggested that different GPCRs may exhibit different

Table 4 Electrostatic contacts between μ and δ receptors in μ(TM1,7)–δ(TM4,5) and μ(TM6,7)–δ(TM4,5) contact patterns

μ(TM1,7)–δ(TM4,5)		μ(TM6,7)–δ(TM4,5)	
μ Receptor[a]	δ Receptor[a]	μ Receptor[a]	δ Receptor[a]
ARG265(IC3)	ASP158(IC2)	ARG265(IC3)	ASP158(IC2)
ARG279(TM6)	ASP158(IC2)	GLU343(H8)	ARG160(IC2)
GLU343(H8)	ARG160(IC2)	GLU395(C-term)	ARG160(IC2)
GLU390(C-term)	ARG160(IC2)		
GLU395(C-term)	ARG160(IC2)		

[a] Residues are numbered according to each receptor

Table 5 Hydrogen bonds between μ and δ receptors in μ(TM1,7)–δ(TM4,5) contact pattern and μ(TM6,7)–δ(TM4,5) contact pattern

μ Receptor[a]		δ Receptor[a]	
Residue	Atom	Residue	Atom
μ(TM1,7)–δ(TM4,5)			
ARG265(IC3)	NH2	ASP158 (IC2)	OD2
GLN316(EC3)	OE1	TRP209(TM5)	O
PHE340(TM7)	O	LYS164(TM4)	NZ
μ(TM6,7)–δ(TM4,5)			
ARG265 (IC3)	NH1	ASP158 (IC2)	OD2
SER319(TM7)	OG	LYS122(TM3)	NZ
SER319(TM7)	OG	MET184(TM4)	O

[a] Residues are numbered according to each receptor

Table 6 Hydrophobic contacts between μ and δ receptors in μ(TM1,7)–δ(TM4,5) and μ(TM6,7)–δ(TM4,5) contact patterns

μ(TM1,7)–δ(TM4,5)		μ(TM6,7)–δ(TM4,5)	
μ Receptor[a]	δ Receptor[a]	μ Receptor[a]	δ Receptor[a]
THR72(TM1)	MET184(TM4)	VAL290(TM6)	VAL174(TM4)
ILE73(TM1)	VAL181(TM4)	VAL293(TM6)	LEU175(TM4)
ILE73(TM1)	VAL185(TM4)	CYS294(TM6)	VAL174(TM4)
LEU76(TM1)	SER177(TM4)	PRO297(TM6)	GLY178(TM4)
LEU76(TM1)	VAL181(TM4)	PRO297(TM6)	PRO182(TM4)
LEU76(TM1)	MET184(TM4)	TYR301(TM6)	TRP209(TM4)
VAL318(TM7)	MET186(TM4)	VAL302(TM6)	VAL185(TM4)
PHE322(TM7)	PRO182(TM4)	LYS305(TM6)	TRP209(TM4)
VAL336(TM7)	LEU167(TM4)	SER319(TM7)	MET184(TM4)
PHE340(TM7)	ALA163(TM4)	PHE322(TM7)	VAL181(TM4)
PHE340(TM7)	LYS164(TM4)	PHE322(TM7)	MET184(TM4)
PHE340(TM7)	LEU167(TM4)	CYS323(TM7)	VAL181(TM4)
THR396(C-term)	ASP364(C-term)	LEU326(TM7)	SER177(TM4)
THR396(C-term)	ALA371(C-term)	LEU326(TM7)	VAL181(TM4)
PRO398(C-term)	ASP364(C-term)	PHE340(TM7)	ALA163(TM4)
		GLU393(C-term)	ARG356(C-term)

[a] Residues are numbered according to each receptor

dimerization interfaces and the symmetric architecture may be favored by the homodimers.

With respect to our predictions, TM4 and TM5 of δ opioid receptor were involved in the two preferred μ–δ heterodimers, and the two heterodimers all represented asymmetric architectures. The asymmetric interface was also observed in dopamine D2–adenosine A2A heterodimer [9]. Based on the chimeric receptor experiment, the interface of the heterodimer was formed in TM5 and TM6 of dopamine D2 receptor and TM4 of adenosine A2A receptor. In addition, the previously mentioned disulfide bridges in TM3 and TM4 of 5HT4 receptor were not involved in the beta2 adrenergic-5HT4 dimerization interface [96]. These evidences seemed to suggest that the intermolecular contact in heterodimer may be different from that of the homodimer, and the asymmetric interface may contribute to the GPCR heterodimerization. However, these possibilities should be examined in the further studies.

Conclusion

In this work, the full-length homology models of μ and δ receptors, and the protein–protein protocols had been used to construct the possible models of the μ–δ heterodimer. The 30 ns molecular dynamics of both monomers provided many reliable conformations to be probed in docking simulation. The predominance contact patterns with larger population in the cluster analysis were further examined by their shape complementary and interaction energy. Statistics showed that the most favorable model was the μ(TM1,7)–δ(TM4,5) contact dimmer, with the interactions more frequently happening between μ(TM1) and δ(TM4), and that the next favorable model was the μ(TM6,7)–δ(TM4,5) contact dimer, with the μ(TM6)–δ(TM4) interaction being dominant. Both contact patterns had close contacts in the C-terminus domains. For δ receptor, the δ-TM4 probably played a primary role in mediating the interaction between the two monomers in heterodimer. For μ receptor, the TM1, 6 and 7 had propensity to participate in the interface, because the TM7 helix packed more inwardly into the transmembrane bundle, TM1 and TM6 tend to had more residues interact with δ receptor. This study was in agreement with previous experimental data and the computational prediction, indicated that our models of the μ–δ heterodimer are well grounded and therefore, was helpful to understand the dimerization mechanism .

Acknowledgments This work was supported by grants from the National Natural Science Foundation of China (Nos. 20772052, 20621091, and 20525206), the Specialized Research Fund for the Doctoral Program in Higher Education Institutions (No. 20060730017), and the Chang Jiang Program of the Ministry of Education of China. The authors thank The High Performance Center of Lanzhou University for providing computational resource.

References

1. Horn F, Bettler E, Oliveira L, Campagne F, Cohen FE, Vriend G (2003) Nucleic Acids Res 31:294. doi:10.1093/nar/gkg103
2. Fredriksson R, Lagerstrom MC, Lundin LG, Schioth HB (2003) Mol Pharmacol 63:1256. doi:10.1124/mol.63.6.1256
3. Kristiansen K (2004) Pharmacol Ther 103:21. doi:10.1016/j.pharmthera.2004.05.002

4. Ma P, Zemmel R (2002) Nat Rev Drug Discov 1:571. doi:10.1038/nrd884
5. Wise A, Gearing K, Rees S (2002) Drug Discov Today 7:235. doi:10.1016/S1359-6446(01)02131-6
6. Drews J (2000) Science 287:1960. doi:10.1126/science.287.5460.1960
7. Hopkins AL, Groom CR (2002) Nat Rev Drug Discov 1:727. doi:10.1038/nrd892
8. Klabunde T, Hessler G (2002) ChemBioChem 3:928. doi:10.1002/1439-7633(20021004)3:10<928::AID-CBIC928>3.0.CO;2-5
9. Canals M, Marcellino D, Fanelli F, Ciruela F, de Benedetti P, Goldberg SR, Neve K, Fuxe K, Agnati LF, Woods AS, Ferre S, Lluis C, Bouvier M, Franco R (2003) J Biol Chem 278:46741. doi:10.1074/jbc.M306451200
10. Bouvier M (2001) Nat Rev Neurosci 2:274. doi:10.1038/35067575
11. Bulenger S, Marullo S, Bouvier M (2005) Trends Pharmacol Sci 26:131. doi:10.1016/j.tips.2005.01.004
12. Fotiadis D, Jastrzebska B, Philippsen A, Muller DJ, Palczewski K, Engel A (2006) Curr Opin Struct Biol 16:252. doi:10.1016/j.sbi.2006.03.013
13. Franco R, Canals M, Marcellino D, Ferre S, Agnati L, Mallol J, Casado V, Ciruela F, Fuxe K, Lluis C, Canela EI (2003) Trends Biochem Sci 28:238. doi:10.1016/S0968-0004(03)00065-3
14. Maggio R, Novi F, Scarselli M, Corsini GU (2005) FEBS J 272:2939. doi:10.1111/j.1742-4658.2005.04729.x
15. Milligan G (2004) Mol Pharmacol 66:1. doi:10.1124/mol.104.000497
16. Milligan G (2006) Drug Discov Today 11:541. doi:10.1016/j.drudis.2006.04.007
17. Park PS, Filipek S, Wells JW, Palczewski K (2004) Biochemistry 43:15643. doi:10.1021/bi047907k
18. Prinster SC, Hague C, Hall RA (2005) Pharmacol Rev 57:289. doi:10.1124/pr.57.3.1
19. Rios CD, Jordan BA, Gomes I, Devi LA (2001) Pharmacol Ther 92:71. doi:10.1016/S0163-7258(01)00160-7
20. Terrillon S, Bouvier M (2004) EMBO Rep 5:30. doi:10.1038/sj.embor.7400052
21. Salahpour A, Angers S, Bouvier M (2000) Trends Endocrinol Metab 11:163. doi:10.1016/S1043-2760(00)00260-5
22. Angers S, Salahpour A, Bouvier M (2002) Annu Rev Pharmacol Toxicol 42:409. doi:10.1146/annurev.pharmtox.42.091701.082314
23. Gazi L, Lopez-Gimenez JF, Strange PG (2002) Curr Opin Drug Discov Dev 5:756
24. Gomes I, Jordan BA, Gupta A, Rios C, Trapaidze N, Devi LA (2001) J Mol Med 79:226. doi:10.1007/s001090100219
25. Lee SP, O'Dowd BF, George SR (2003) Life Sci 74:173. doi:10.1016/j.lfs.2003.09.028
26. Liang Y, Fotiadis D, Filipek S, Saperstein DA, Palczewski K, Engel A (2003) J Biol Chem 278:21655. doi:10.1074/jbc.M302536200
27. Fotiadis D, Liang Y, Filipek S, Saperstein DA, Engel A, Palczewski K (2003) Nature 421:127. doi:10.1038/421127a
28. Reddy PS, Corley RB (1998) Bioessays 20:546. doi:10.1002/(SICI)1521-1878(199807)20:7<546::AID-BIES5>3.0.CO;2-I
29. Chen Y, Mestek A, Liu J, Yu L (1993) Biochem J 295(Pt 3):625
30. Waldhoer M, Bartlett SE, Whistler JL (2004) Annu Rev Biochem 73:953. doi:10.1146/annurev.biochem.73.011303.073940
31. Wang D, Sun X, Bohn LM, Sadee W (2005) Mol Pharmacol 67:2173. doi:10.1124/mol.104.010272
32. George SR, Fan T, Xie Z, Tse R, Tam V, Varghese G, O'Dowd BF (2000) J Biol Chem 275:26128. doi:10.1074/jbc.M000345200
33. Gomes I, Jordan BA, Gupta A, Trapaidze N, Nagy V, Devi LA (2000) J Neurosci 20:RC110
34. Jordan BA, Devi LA (1999) Nature 399:697. doi:10.1038/21441
35. Ananthan S, Kezar HSIII, Carter RL, Saini SK, Rice KC, Wells JL, Davis P, Xu H, Dersch CM, Bilsky EJ, Porreca F, Rothman RB (1999) J Med Chem 42:3527. doi:10.1021/jm990039i
36. Daniels DJ, Lenard NR, Etienne CL, Law PY, Roerig SC, Portoghese PS (2005) Proc Natl Acad Sci USA 102:19208. doi:10.1073/pnas.0506627102
37. Gomes I, Gupta A, Filipovska J, Szeto HH, Pintar JE, Devi LA (2004) Proc Natl Acad Sci USA 101:5135. doi:10.1073/pnas.0307601101
38. Schiller PW, Fundytus ME, Merovitz L, Weltrowska G, Nguyen TM, Lemieux C, Chung NN, Coderre TJ (1999) J Med Chem 42:3520. doi:10.1021/jm980724+
39. Wells JL, Bartlett JL, Ananthan S, Bilsky EJ (2001) J Pharmacol Exp Ther 297:597
40. Waldhoer M, Fong J, Jones RM, Lunzer MM, Sharma SK, Kostenis E, Portoghese PS, Whistler JL (2005) Proc Natl Acad Sci USA 102:9050. doi:10.1073/pnas.0501112102
41. Okada T, Sugihara M, Bondar AN, Elstner M, Entel P, Buss V (2004) J Mol Biol 342:571. doi:10.1016/j.jmb.2004.07.044
42. Hillisch A, Pineda LF, Hilgenfeld R (2004) Drug Discov Today 9:659. doi:10.1016/S1359-6446(04)03196-4
43. Baldwin JM, Schertler GF, Unger VM (1997) J Mol Biol 272:144
44. Ballesteros J, Palczewski K (2001) Curr Opin Drug Discov Dev 4:561. doi:10.1006/jmbi.1997.1240
45. Surratt CK, Adams WR (2005) Curr Top Med Chem 5:315. doi:10.2174/1568026053544533
46. Russell RB, Alber F, Aloy P, Davis FP, Korkin D, Pichaud M, Topf M, Sali A (2004) Curr Opin Struct Biol 14:313. doi:10.1016/j.sbi.2004.04.006
47. Smith GR, Sternberg MJ (2002) Curr Opin Struct Biol 12:28. doi:10.1016/S0959-440X(02)00285-3
48. Valencia A, Pazos F (2002) Curr Opin Struct Biol 12:368. doi:10.1016/S0959-440X(02)00333-0
49. Dean MK, Higgs C, Smith RE, Bywater RP, Snell CR, Scott PD, Upton GJ, Howe TJ, Reynolds CA (2001) J Med Chem 44:4595. doi:10.1021/jm010290+
50. Vohra S, Chintapalli SV, Illingworth CJ, Reeves PJ, Mullineaux PM, Clark HS, Dean MK, Upton GJ, Reynolds CA (2007) Biochem Soc Trans 35:749. doi:10.1042/BST0350749
51. Jones DT, Taylor WR, Thornton JM (1992) Nature 358:86. doi:10.1038/358086a0
52. Fiser A, Sali A (2003) Methods Enzymol 374:461. doi:10.1016/S0076-6879(03)74020-8
53. Kuhlman B, Dantas G, Ireton GC, Varani G, Stoddard BL, Baker D (2003) Science 302:1364. doi:10.1126/science.1089427
54. Jones DT (1999) J Mol Biol 292:195. doi:10.1006/jmbi.1999.3091
55. Lemer CMR, Rooman MJ, Wodak SJ (1995) Proteins-Structure Funct Genet 23:337. doi:10.1002/prot.340230308
56. Murzin AG (1999) Proteins: Struct Funct Genet Suppl 3:88. doi:0.1002/(SICI)1097-0134(1999)37:3+<88::AID-PROT13>3.0.CO;2-3
57. Sippl MJ, Lackner P, Domingues FS, Prlic A, Malik R, Andreeva A, Wiederstein M (2001) Proteins: Struct Funct Genet 5:55
58. Fanelli F, Menziani C, Scheer A, Cotecchia S, De Benedetti PG (1998) Methods 14:302. doi:10.1006/meth.1998.0586
59. Tusnady GE, Simon I (1998) J Mol Biol 283:489. doi:10.1006/jmbi.1998.2107
60. Tusnady GE, Simon I (2001) Bioinformatics 17:849. doi:10.1093/bioinformatics/17.9.849
61. Claros MG, von Heijne G (1994) Comput Appl Biosci 10:685
62. von Heijne G (1992) J Mol Biol 225:487. doi:10.1016/0022-2836(92)90934-C
63. Hofmann K, Stoffel W (1993) Biol Chem Hoppe Seyler 374:166
64. Berman HM, Westbrook J, Feng Z, Gilliland G, Bhat TN, Weissig H, Shindyalov IN, Bourne PE (2000) Nucleic Acids Res 28:235. doi:10.1093/nar/28.1.235

65. Altschul SF, Madden TL, Schaffer AA, Zhang J, Zhang Z, Miller W, Lipman DJ (1997) Nucleic Acids Res 25:3389. doi:10.1093/nar/25.17.3389
66. Laskowski RA, Macarthur MW, Moss DS, Thornton JM (1993) J Appl Cryst 26:283. doi:10.1107/S0021889892009944
67. Berendsen HJ, Vanderspoel D, Vandrunen R (1995) Comput Phys Commun 91:43. doi:10.1016/0010-4655(95)00042-E
68. Vanbuuren AR, Marrink SJ, Berendsen HJC (1993) J Phys Chem 97:9206. doi:10.1021/j100138a023
69. Berger O, Edholm O, Jahnig F (1997) Biophys J 72:2002. doi:10.1016/S0006-3495(97)78845-3
70. Tieleman DP, Berendsen HJ, Sansom MS (1999) Biophys J 76:1757. doi:10.1016/S0006-3495(99)77337-6
71. Tieleman DP, Sansom MS, Berendsen HJ (1999) Biophys J 76:40. doi:10.1016/S0006-3495(99)77176-6
72. Darden T, York D, Pedersen L (1993) J Chem Phys 98:10089. doi:10.1063/1.464397
73. Hess B, Bekker H, Berendsen HJC, Fraaije J (1997) J Comput Chem 18:1463. doi:10.1002/(SICI)1096-987X(199709)18:12<1463::AID-JCC4>3.0.CO;2-H
74. Berendsen HJC, Postma JPM, Vangunsteren WF, Dinola A, Haak JR (1984) J Chem Phys 81:3684. doi:10.1063/1.448118
75. Chen R, Weng ZP (2003) Proteins-Structure Funct Genet 51:397. doi:10.1002/prot.10334
76. Casciari D, Seeber M, Fanelli F (2006) BMC Bioinformatics 7:340
77. Mihel J, Sikic M, Tomic S, Jeren B, Vlahovicek K (2008) BMC Struct Biol 8:21. doi:10.1186/1472-6807-8-21
78. DeLano WL (2002) The PyMOL molecular graphics system. DeLano Scientific, Palo Alto
79. Kobilka B, Schertler GF (2008) Trends Pharmacol Sci 29:79. doi:10.1016/j.tips.2007.11.009
80. Cherezov V, Rosenbaum DM, Hanson MA, Rasmussen SG, Thian FS, Kobilka TS, Choi HJ, Kuhn P, Weis WI, Kobilka BK, Stevens RC (2007) Science 318:1258. doi:10.1126/science.1150577
81. Fanelli F, De Benedetti PG (2005) Chem Rev 105:3297. doi:10.1021/cr000095n
82. Visiers I, Ballesteros JA, Weinstein H (2002) Methods Enzymol 343:329. doi:10.1016/S0076-6879(02)43145-X
83. Palczewski K, Kumasaka T, Hori T, Behnke CA, Motoshima H, Fox BA, Le Trong I, Teller DC, Okada T, Stenkamp RE, Yamamoto M, Miyano M (2000) Science 289:739. doi:10.1126/science.289.5480.739
84. Huang P, Li J, Chen C, Visiers I, Weinstein H, Liu-Chen LY (2001) Biochemistry 40:13501. doi:10.1021/bi010917q
85. Huang P, Visiers I, Weinstein H, Liu-Chen LY (2002) Biochemistry 41:11972. doi:10.1021/bi026067b
86. Spivak CE, Beglan CL, Seidleck BK, Hirshbein LD, Blaschak CJ, Uhl GR, Surratt CK (1997) Mol Pharmacol 52:983
87. Surratt CK, Johnson PS, Moriwaki A, Seidleck BK, Blaschak CJ, Wang JB, Uhl GR (1994) J Biol Chem 269:20548
88. Comeau SR, Gatchell DW, Vajda S, Camacho CJ (2004) Nucleic Acids Res 32:W96. doi:10.1093/nar/gkh354
89. Fan T, Varghese G, Nguyen T, Tse R, O'Dowd BF, George SR (2005) J Biol Chem 280:38478. doi:10.1074/jbc.M505644200
90. Krol M, Tournier AL, Bates PA (2007) Proteins 68:159. doi:10.1002/prot.21391
91. Filizola M, Olmea O, Weinstein H (2002) Protein Eng 15:881. doi:10.1093/protein/15.11.881
92. Jones S, Thornton JM (1997) J Mol Biol 272:121. doi:10.1006/jmbi.1997.1234
93. Keskin O, Gursoy A, Ma B, Nussinov R (2008) Chem Rev 108:1225. doi:10.1021/cr040409x
94. Lodowski DT, Salom D, Le Trong I, Teller DC, Ballesteros JA, Palczewski K, Stenkamp RE (2007) J Struct Biol 158:455. doi:10.1016/j.jsb.2007.01.017
95. Guo W, Shi L, Javitch JA (2003) J Biol Chem 278:4385. doi:10.1074/jbc.C200679200
96. Berthouze M, Rivail L, Lucas A, Ayoub MA, Russo O, Sicsic S, Fischmeister R, Berque-Bestel I, Jockers R, Lezoualc'h F (2007) Biochem Biophys Res Commun 356:642. doi:10.1016/j.bbrc.2007.03.030
97. Mancia F, Assur Z, Herman AG, Siegel R, Hendrickson WA (2008) EMBO Rep 9:363. doi:10.1038/embor.2008.27